Recent Two-Fluid Results with NIMROD

C. R. Sovinec,[1] J. R. King,[2] J. B. O'Bryan,[1] J. P. Sauppe,[1] and D. D. Schnack[1]

[1]*University of Wisconsin-Madison*

[2] *Tech-X Corporation*

US-Japan JIFT Workshop on "Recent studies of extended MHD and MHD simulations"

November 9-10, 2013   Denver, Colorado

Outline

- Introduction and motivation
- Verification of ion temperature-gradient instability (ITG)
- Verification of drift-tearing
- Two-fluid relaxation in reversed-field pinches (RFPs)
- Non-inductive startup in the Pegasus spherical torus
- Concluding remarks

Introduction: Extended-MHD modeling is needed for predictive simulation of macroscopic dynamics in magnetically confined plasma.

- ITER and future large experiments require avoidance or control of macroscopic dynamics.

- Disruption, ELMs, islands, and sawteeth would reduce performance or damage the device.

- Resistive-MHD misses many effects.

High-β disruption, Kruger

ELM evolution

Sawtooth cycle
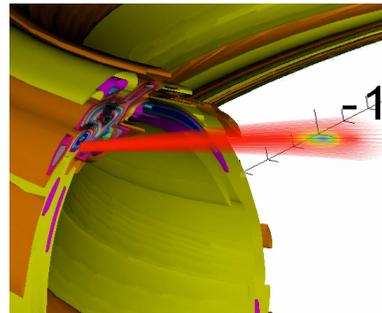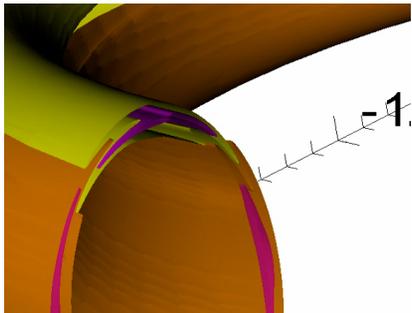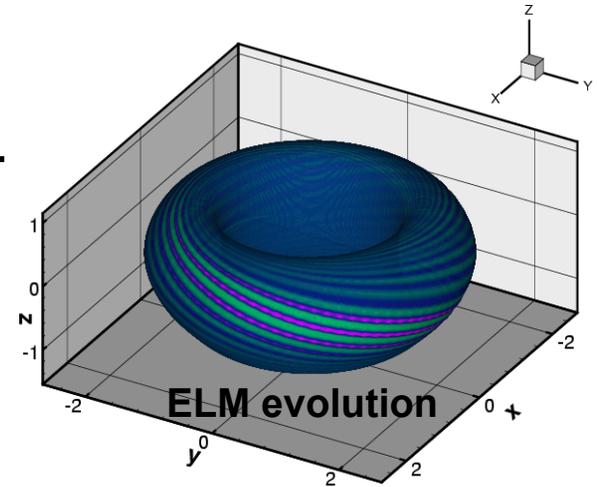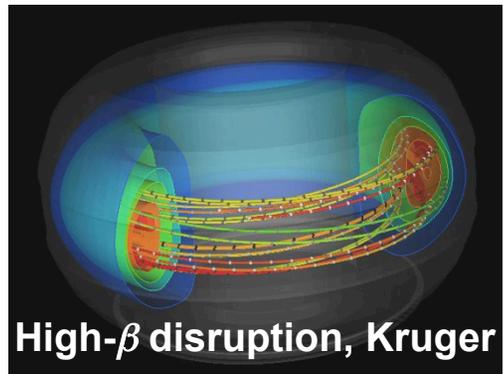
Island suppression with RF, Jenkins
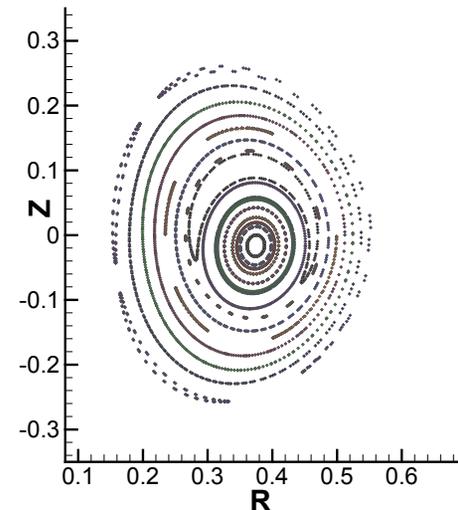
Solving low-frequency two-fluid systems incorporates drift and fast-reconnection effects.

$$\frac{\partial n}{\partial t} = -\nabla \cdot \left(n\mathbf{V} - D_n \nabla n + D_h \nabla \nabla^2 n \right)$$

$$mn\left(\frac{\partial}{\partial t}\mathbf{V} + \mathbf{V} \cdot \nabla \mathbf{V} \right) = \mathbf{J} \times \mathbf{B} - \nabla p + \nabla \cdot \underline{\underline{\Pi}}$$

$$\frac{2n}{3}\left(\frac{\partial}{\partial t}T_e + \mathbf{V}_e \cdot \nabla T_e \right) = -nT_e \nabla \cdot \mathbf{V}_e + \nabla \cdot \mathbf{q}_e + n\sigma\left(T_i - T_e \right) + \eta J^2$$

$$\frac{2n}{3}\left(\frac{\partial}{\partial t}T_i + \mathbf{V}_i \cdot \nabla T_i \right) = -nT_i \nabla \cdot \mathbf{V}_i + \nabla \cdot \mathbf{q}_i + n\sigma\left(T_e - T_i \right) + Q_i$$

$$\frac{\partial}{\partial t}\mathbf{B} = -\nabla \times \left[\eta\mathbf{J} - \mathbf{V} \times \mathbf{B} + \frac{1}{ne}\left(\mathbf{J} \times \mathbf{B} - \nabla p_e + \frac{m_e}{e}\frac{\partial}{\partial t}\mathbf{J} \right) \right]$$

$$\mathbf{J} = \mu_0^{-1}\nabla \times \mathbf{B}$$

- Two-fluid effects are included in Ohm's law (blue), and first-order FLR effects appear in closure relations (red).
- Diffusive particle fluxes (green) are numerical.

Closure relations represent lowest-order FLR and collisional effects.

- Stress tensor $\underline{\mathbf{\Pi}}$ for collisional plasma is a combination of $\underline{\mathbf{\Pi}}_{\mathrm{gv}}$, $\underline{\mathbf{\Pi}}_\parallel$, and $\underline{\mathbf{\Pi}}_\perp$:

$$\underline{\mathbf{\Pi}}_{\mathrm{gv}} = \frac{m_i p_i}{4eB}\left[\hat{\mathbf{b}}\times\underline{\mathbf{W}}\cdot\left(\underline{\mathbf{I}}+3\hat{\mathbf{b}}\hat{\mathbf{b}}\right)-\left(\underline{\mathbf{I}}+3\hat{\mathbf{b}}\hat{\mathbf{b}}\right)\cdot\underline{\mathbf{W}}\times\hat{\mathbf{b}}\right] \qquad \underline{\mathbf{W}}\equiv\nabla\mathbf{V}+\nabla\mathbf{V}^T-(2/3)(\nabla\cdot\mathbf{V})\underline{\mathbf{I}}$$

$$\underline{\mathbf{\Pi}}_\parallel = \frac{p_i\tau_i}{2}\left(\hat{\mathbf{b}}\cdot\underline{\mathbf{W}}\cdot\hat{\mathbf{b}}\right)\left(\underline{\mathbf{I}}-3\hat{\mathbf{b}}\hat{\mathbf{b}}\right)$$

$$\underline{\mathbf{\Pi}}_\perp \sim -\frac{3p_i m_i^2}{10e^2 B^2\tau_i}\underline{\mathbf{W}} \quad \text{has been treated as} \quad -nm_i\nu_{iso}\underline{\mathbf{W}} \quad \text{or} \quad -nm_i\nu_{kin}\nabla\mathbf{V}$$

- Heat flux density is mostly parallel and diamagnetic, but some perpendicular diffusion helps numerics:

$$\mathbf{q}_i = -\left[\kappa_{\parallel_i}\hat{\mathbf{b}}\hat{\mathbf{b}}+\kappa_{\perp_i}\left(\underline{\mathbf{I}}-\hat{\mathbf{b}}\hat{\mathbf{b}}\right)-\frac{5}{2}\frac{nT_i}{eB}\hat{\mathbf{b}}\times\underline{\mathbf{I}}\right]\cdot\nabla T_i$$

$$\mathbf{q}_e = -\left[\kappa_{\parallel_e}\hat{\mathbf{b}}\hat{\mathbf{b}}+\kappa_{\perp_e}\left(\underline{\mathbf{I}}-\hat{\mathbf{b}}\hat{\mathbf{b}}\right)+\frac{5}{2}\frac{nT_e}{eB}\hat{\mathbf{b}}\times\underline{\mathbf{I}}\right]\cdot\nabla T_e$$

- We numerically solve this system and various subsets with the NIMROD code [https://nimrodteam.org; algorithm: JCP **229**, 5803 (2010)].

ITG Verification: The fluid limit is represented by extended-MHD that includes diamagnetic drift flows & heat flux densities and ion gyroviscous stress.

- ITG instability requires FLR effects; it is stable in ideal- and resistive-MHD.

- For some applications of extended-MHD modeling, ITG instability [Coppi, PF **10**, 582 (1967)] may be a parasitic effect that hinders a study.

- Here, we summarize verification of slab-geometry ITG [Schnack, *et al.,* PoP **20**, 062106 (2013)], leaving open the question of how to deal with drift-wave instabilities in simulations of sawteeth, tearing, etc.

- The equilibrium has no magnetic shear, and number-density and electron-temperature profiles are uniform.

- Fluid NIMROD computations and Lorentz-ion kinetic computations [Cheng, JCP **245**, 364 (2013)] use

$$T_{i0}(x) = T_{i0}(0)\left[1 + 0.9\tanh\left(x/L_{T_{i0}}\right)\right]$$

Eigenvalues from global fluid computation and analytical results from local approximation agree at small ρ_i / L_{Ti}.

- Instability in the analytical fluid dispersion relation is determined by a single parameter g being greater than unity.

$$g \equiv (27/4)\beta_e^2 \beta_i (\beta_e + 5\beta_i/3)^{-3} k_\perp^2 k_\parallel^{-2} \rho_i^2 L_{Ti}^{-2}$$

- Electron thermal energy is also required for instability.
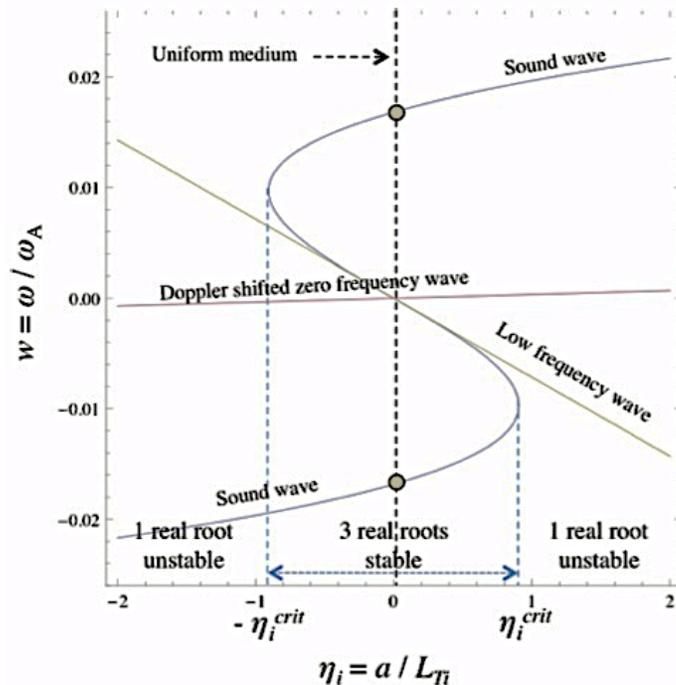
Real frequencies from analytical dispersion relation.
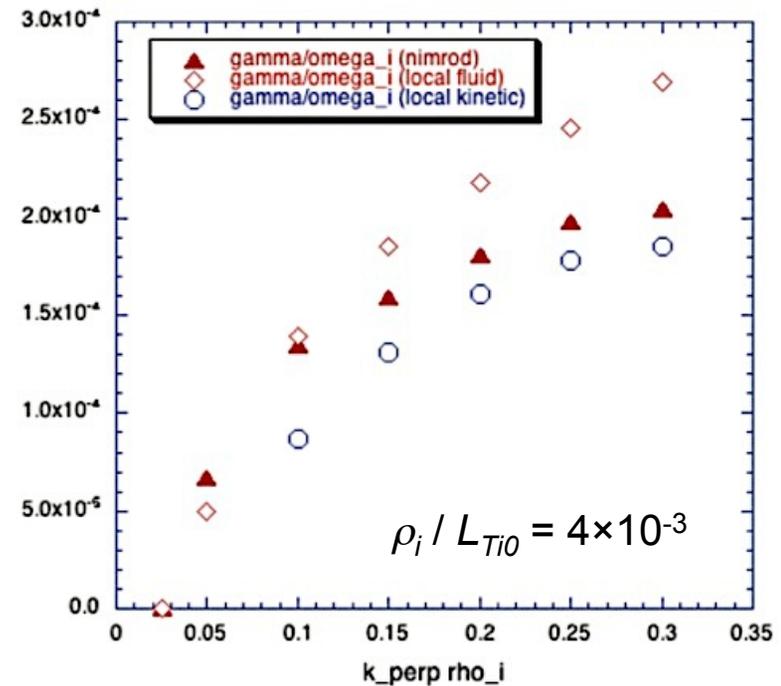
Comparison of NIMROD results with fluid and kinetic analytics [Schnack].

Comparison with global kinetic results emphasizes limitations.
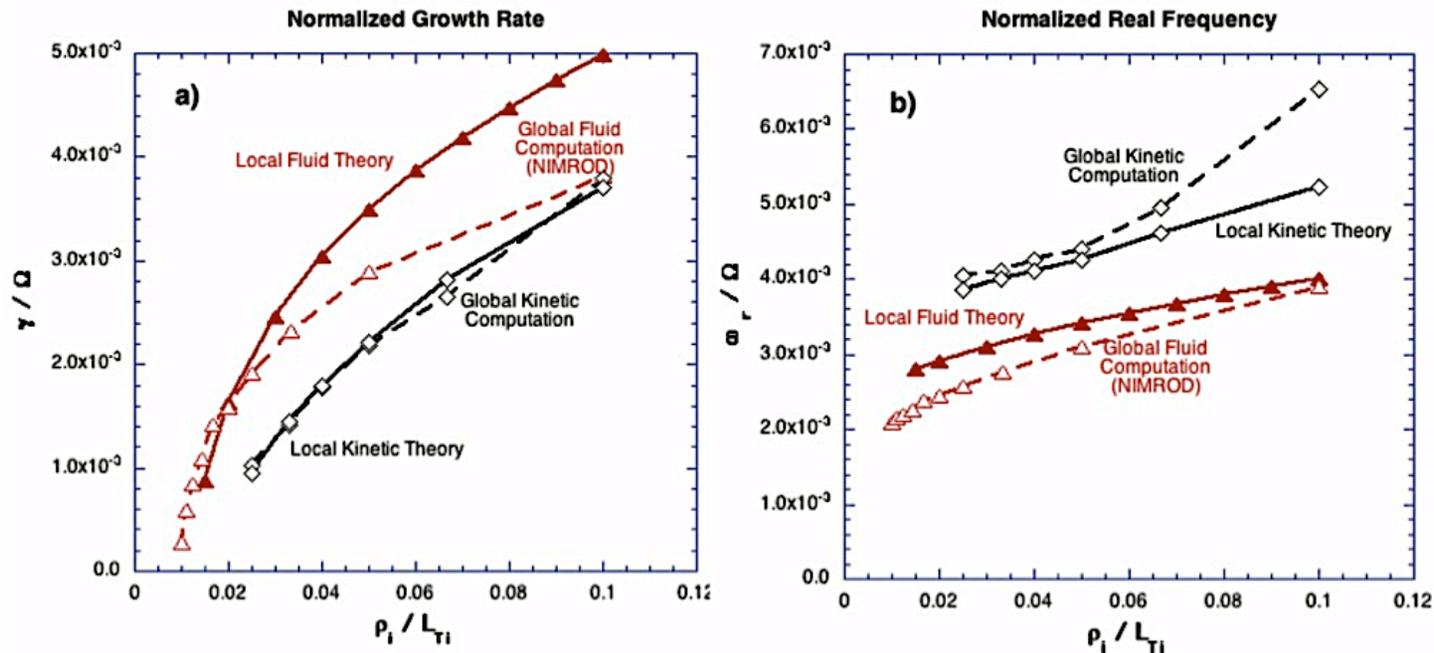
Growth rates and real frequencies from local, analytical dispersion relations and from global fluid and kinetic computation; $k_{perp}\rho_i$=0.2 and $k_{||}/k_{perp}$=0.01 [Schnack, *et al.*, PoP 20, 062106 (2013)].

- Local and global fluid results converge near the marginal stability point.
- Local and global kinetic results are in agreement over a wider range of ρ_i / L_{Ti0}.
- The $k_{perp}\rho_i$-value facilitates kinetic computation, but it is marginal for fluid approximation.

Conclusions from ITG Study

- The ion temperature gradient instability, and likely other drift-wave instabilities, is represented in extended-MHD models used for macroscopic dynamics.

- Local- and global-fluid and local-kinetic results are within a factor of 2 for $k_{perp}\rho_i < 0.2$.

- Scanning ρ_i / L_{Ti0} indicates that the limit of fluid validity is approximately 1/100 in this parameter.

- Unlike kinetic models, fluid models do not have stabilizing effects for large $k_{perp}\rho_i$. This is an important consideration for nonlinear simulation of macroscopic dynamics.

Drift-Tearing Verification: Considering the different regimes in parameter space is important.
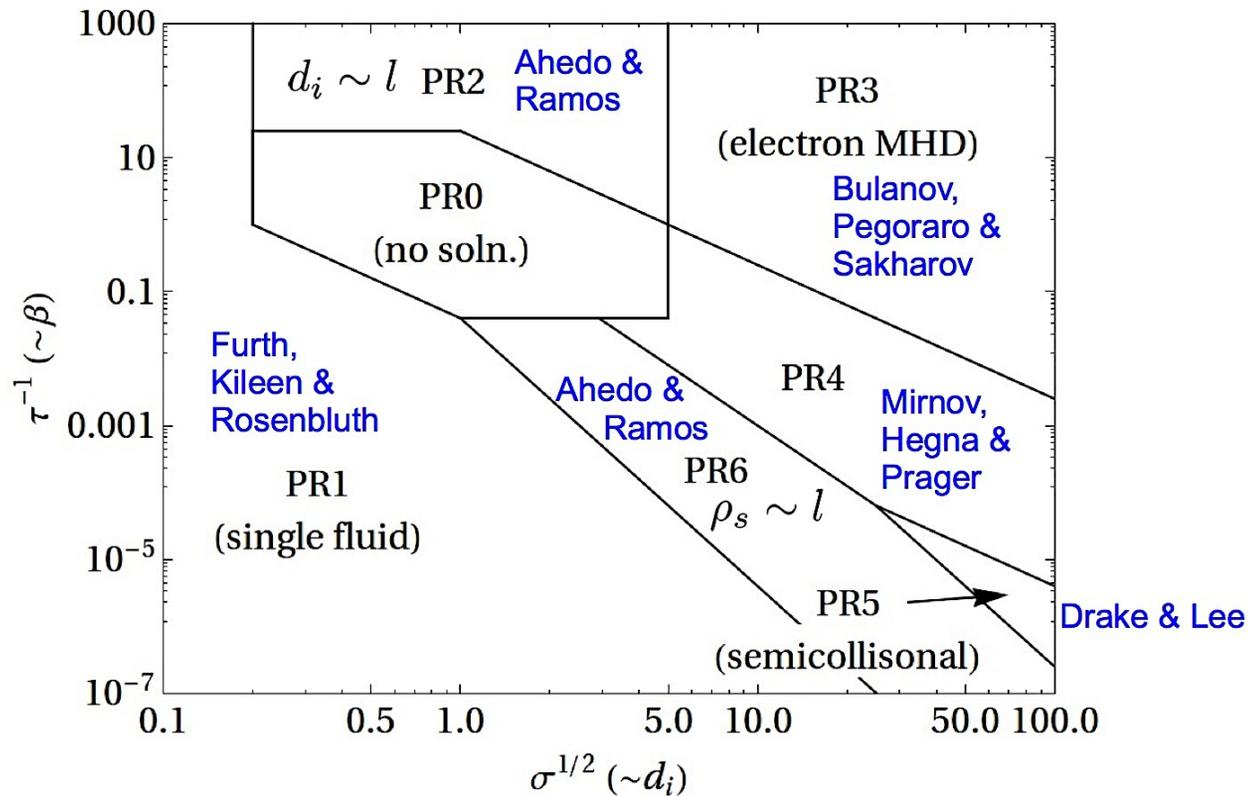
- Mirnov, Hegna, & Prager [PoP **11**, 4468 (2004)] and Ahedo & Ramos [PPCF **51**, 055018 (2009)] categorize two-fluid tearing without drift.
- Ahedo and Ramos characterize the inner layer response by two dimensionless parameters, $\sigma \sim d_i$ and $\tau \sim 1 / \beta$.

Recent analytics aims to evaluate drift-tearing dispersion relations in MFE-application regimes.
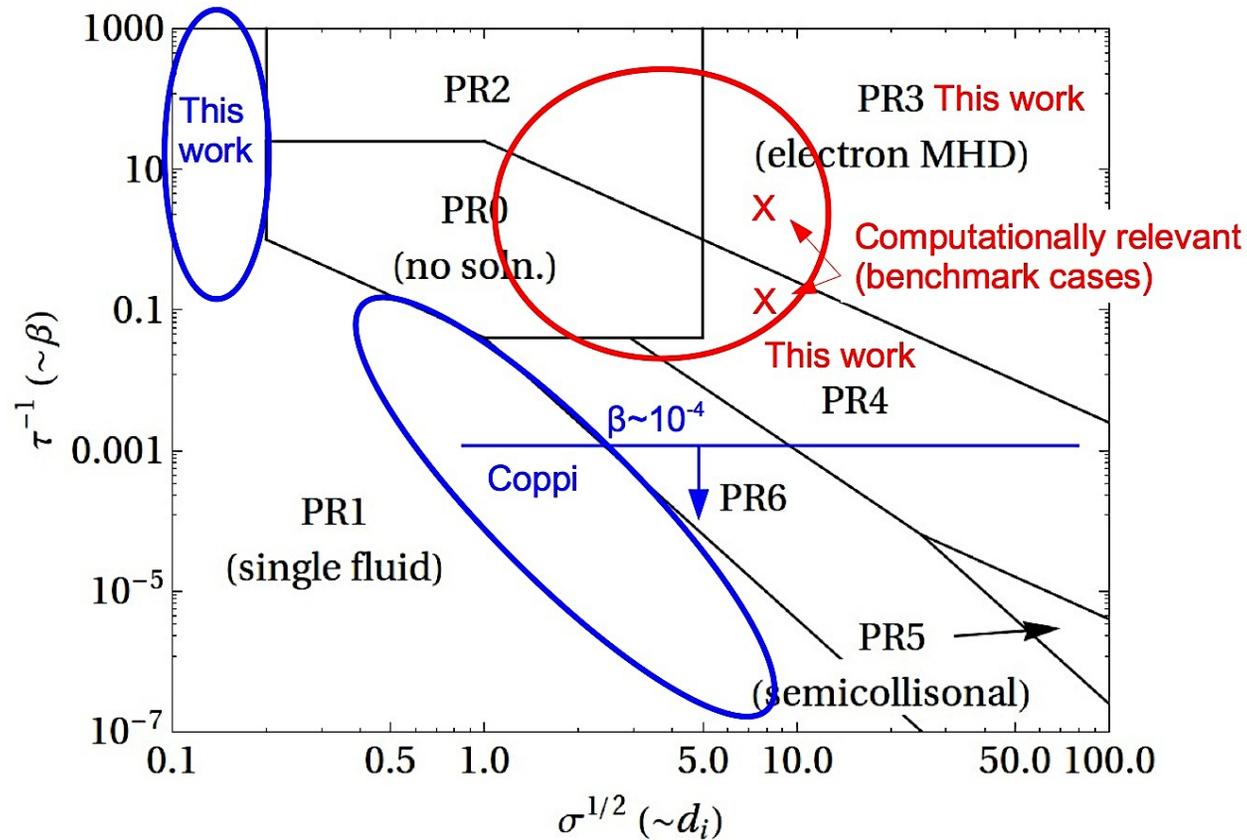
- Analysis by King solved the dispersion relation for moderate-β, small-d_i and now focuses on relevant moderate-β, moderate-d_i regimes.

- Ions are considered to be cold.

- Slab geometry is used, and the pressure profile varies like tanh(x).

For small-d_i, the simplest dispersion relation is formally valid in the small-drift limit, yet initial-value results agree over a broader range of the drift parameter.
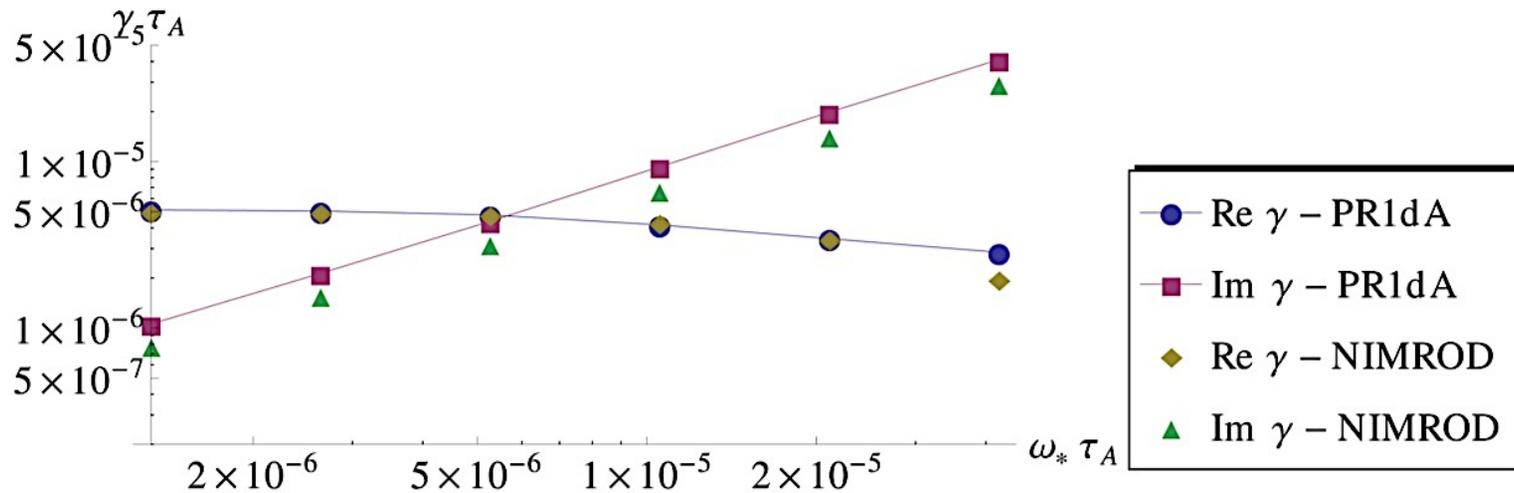
Initial-value computations with NIMROD agree with analytical results (using simplifications for the limit of small drift) in the small-d_i regime. [http://w3.pppl.gov/cemm/Madison2012/King.pdf]

Both physical and numerical questions arise when comparing in the more realistic moderate-d_i regime.
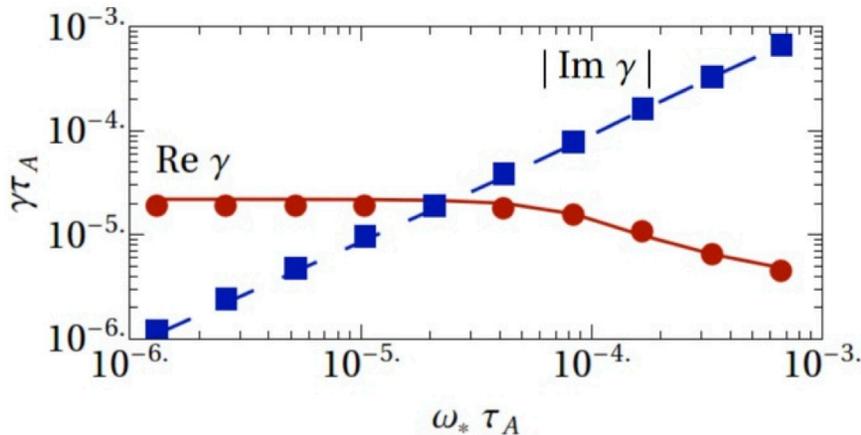
Comparison in the PR4 transition region between electron-MHD and the semi-collisional regime.
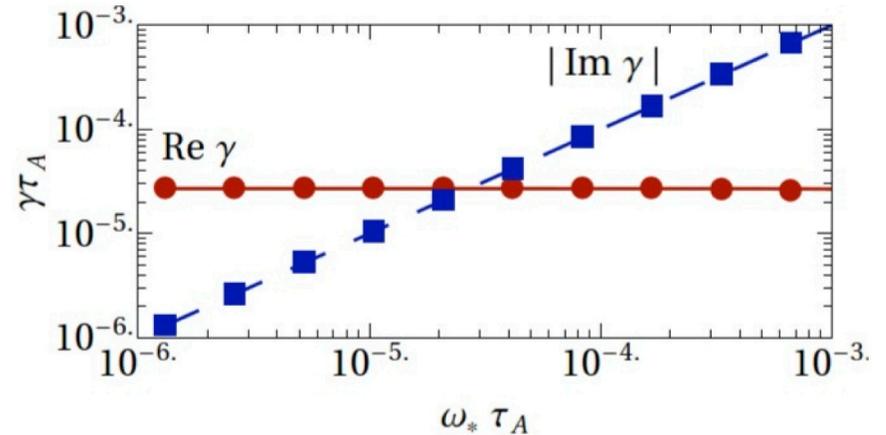
Comparison for electron-MHD. Symbols show NIMROD results, and lines are analytical.

[https://nimrodteam.org/meetings/team_mtg_8_13/JKing_Drift_Tearing.pdf]

- There is good agreement between analytics and computation in both regimes.
- Diamagnetic heat fluxes are important in regimes PR4-5 but have been numerically problematic in PR4 cases.
- No drift stabilization occurs in electron-MHD, but the large-ρ_i conditions may be outside the scope of fluid approximations.

Conclusions from Drift-Tearing Study

- Although we have known about drift-tearing since the 1960s, dispersion relations for many relevant regimes are the subject of current analytical work.

- Apart from diamagnetic heat flux density, our initial-value computations have been validated in several drift-tearing (and non-drifting two-fluid tearing) regimes.

- Similar to ITG, quantitative accuracy may require ion kinetic effects.

Two-Fluid RFP Relaxation: Measurements on MST indicate two-fluid effects during relaxation events.

• In standard MST operation, magnetic relaxation occurs during discrete sawtooth events.

• Laser polarimetry measurements of δj_ϕ for the (1,6) mode, and fitted $\delta \mathbf{b}$ profiles show a correlation that implies significant Hall dynamo. [Ding, *et al.*, PoP **13**, 112306].

• MST parameters have ion-sound-gyroradius ($\rho_s = c_s/\Omega_i$) comparable to the resistive skin depth, so two-fluid linear tearing effects are expected [Mirnov, *et al.*, PoP **11**, 4468, for example].

$$< \delta J \times \delta B >_{//} / n_e e$$

[V/m]

60

40

20

0

0.4   0.8

r/a
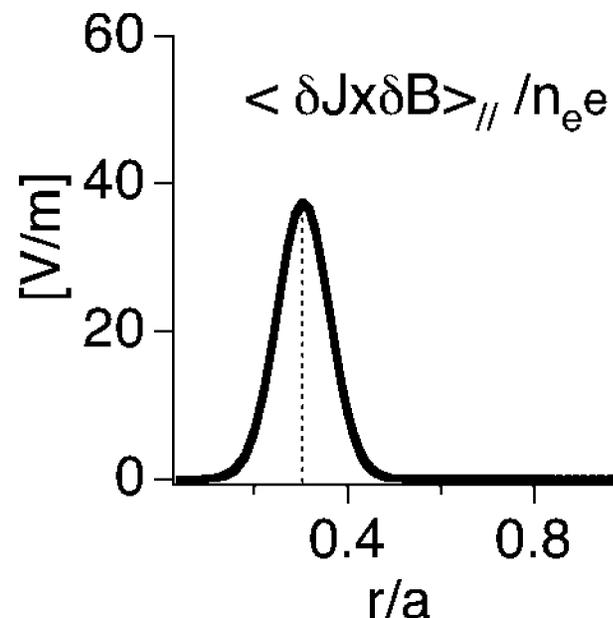
Hall dynamo from (1,6) mode, inferred with multi-chord laser polarimetry measurements on MST.

Probe measurements from MST's edge plasma also show two-fluid effects.

• The existence of Hall dynamo and net parallel Lorentz force density from fluctuations are essentially equivalent.

• Kuritsyn, *et al.*, used an array of magnetic coil triplets to measure Maxwell-stress profiles in the edge of MST [PoP **16**, 55903].

• The group also found Reynolds stress contributions from flow fluctuations, measured by Mach probes.

• The effects largely cancel, but the parallel flow profile tends to flatten.
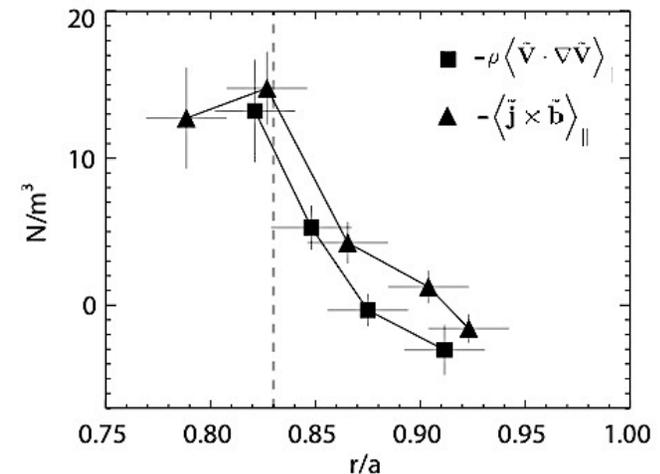
Fluctuation-induced Lorentz and inertial force densities measured during a relaxation event.
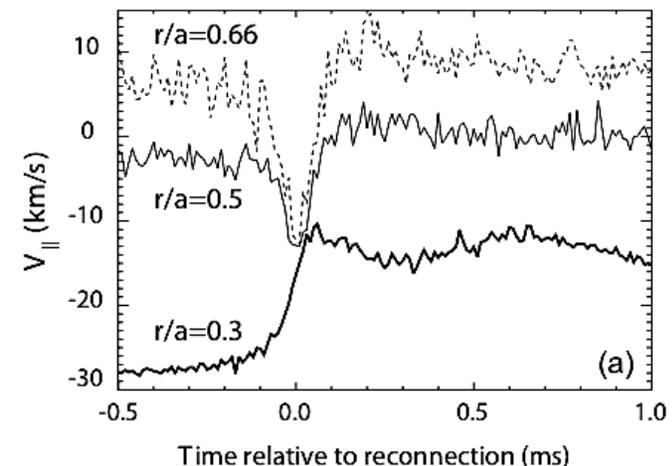
Temporal evolution of parallel flow at three radii in MST.

Two-fluid multi-helicity computations with (ρ_s/a)-values relevant to MST exhibit Hall dynamo during relaxation.
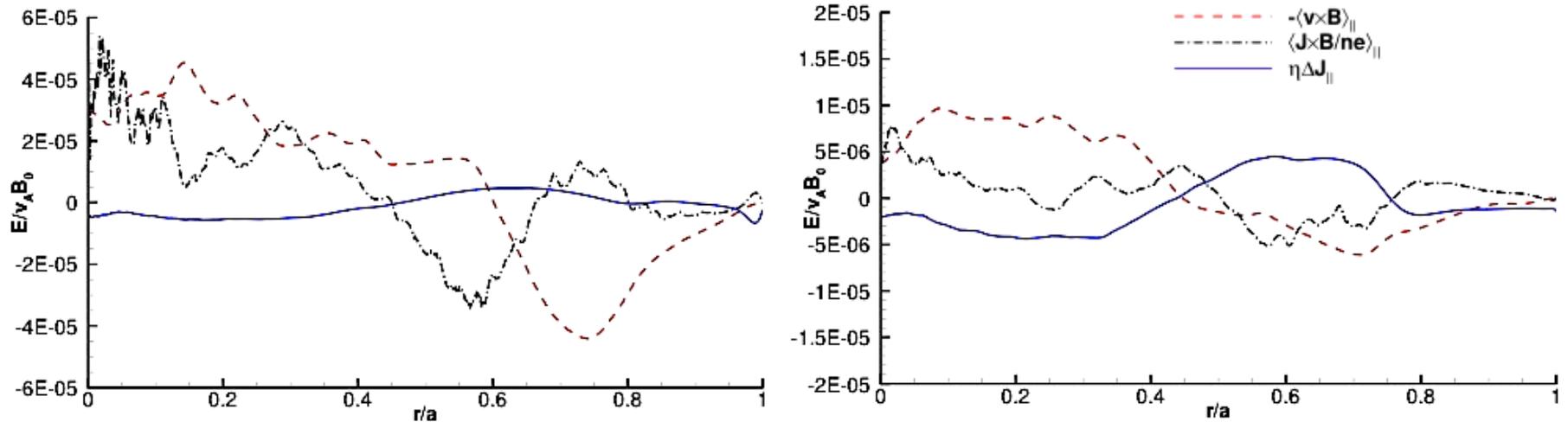
Hall dynamo $n^{-1}e^{-1}\langle \tilde{\mathbf{j}} \times \tilde{\mathbf{b}} \rangle$ is evident and comparable in magnitude to the MHD dynamo $-\langle \tilde{\mathbf{v}} \times \tilde{\mathbf{b}} \rangle$ during the initial (left) and a subsequent (right) relaxation event.

- Our computations at ion sound gyroradius (c_s/Ω_i) $\rho_s=0.05a$ show significant Hall and MHD dynamo effects that are comparable in magnitude during a relaxation event. [King, PoP **19**, 055905 (2012).]

- As in single-fluid computation, the combined dynamo emf acts to reduce parallel current in the core and drive it near the edge.

- Other parameters in the computation are S=80,000, Pm=1, and uniform equilibrium pressure.

Computations with background flow show coupling of magnetic-field and parallel-flow evolution.

Two-Fluid with Warm Ions, J.B>0

Two-Fluid with Warm Ions, J.B<0
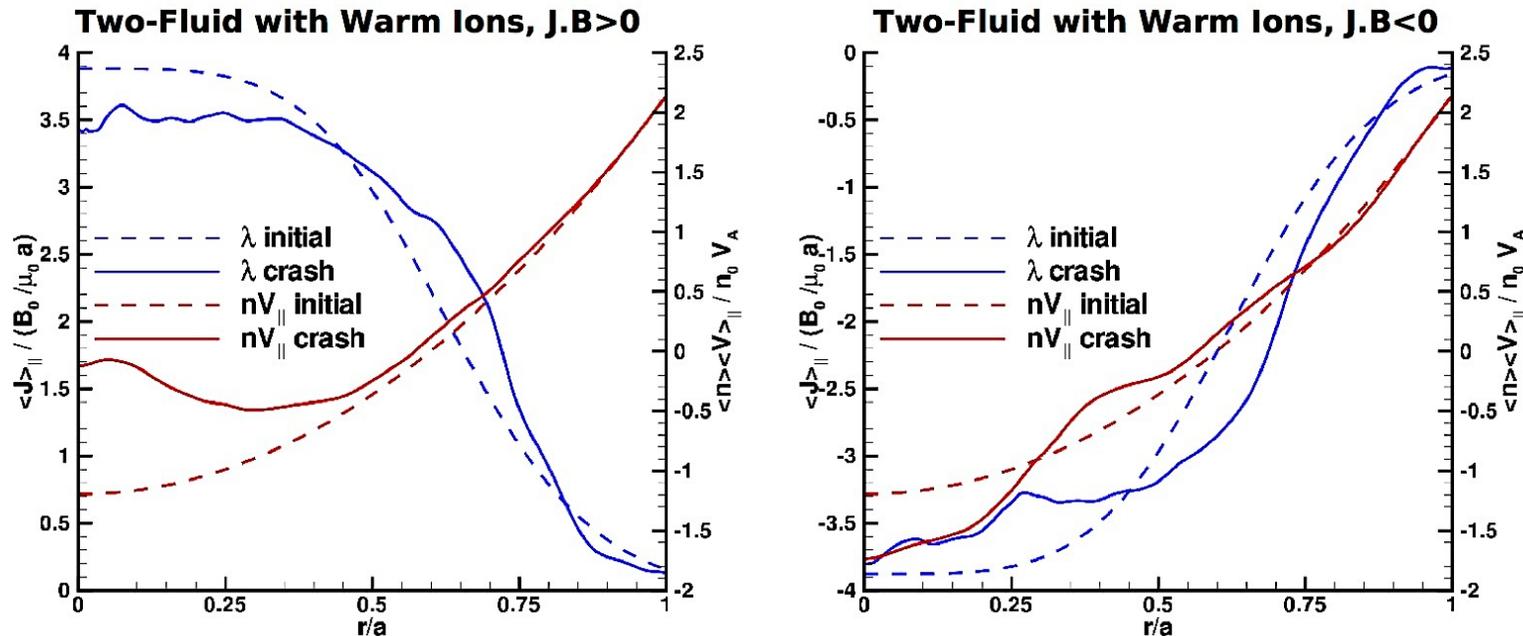
- Lorentz force density associated with the Hall dynamo exceeds the force density from Reynolds stress, independent of current/field/flow orientation.
- In contrast, experimental observations always show flow-profile flattening during relaxation events.
- Computations shown here have S=20,000.

Relative to magnetic energy, computed species helicities are conserved.

- Conserving $K_s = \int \mathbf{A}_s \cdot \nabla \times \mathbf{A}_s \, dVol$ for each species s while minimizing energy predicts $\mathbf{J}_0 = \lambda_1 \mathbf{B}_0$ and $n_0 e \mathbf{V}_0 = \lambda_2 \mathbf{B}_0$ with λ_1 and λ_2 being constants. [Hegna, PoP **5**, 2257 (1998)].

- Here, $\mathbf{A}_s \equiv \mathbf{A} + (m_s/q_s) \mathbf{V}_s$, and K_e is approximately magnetic helicity.
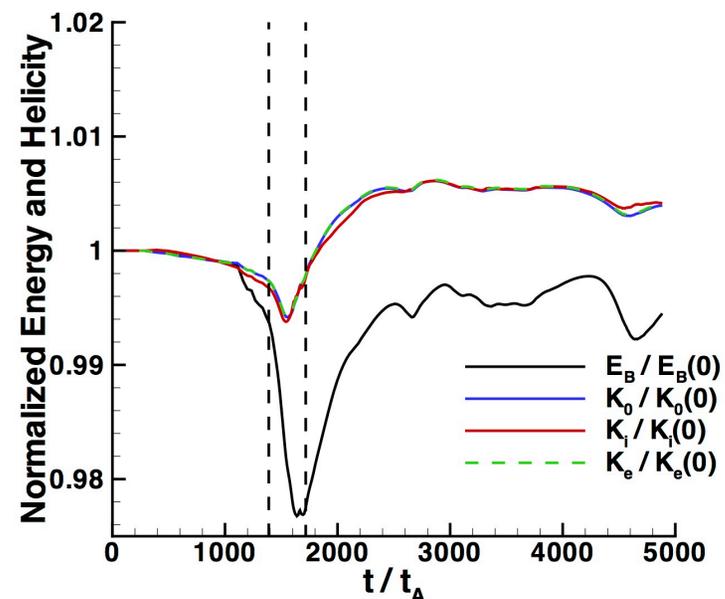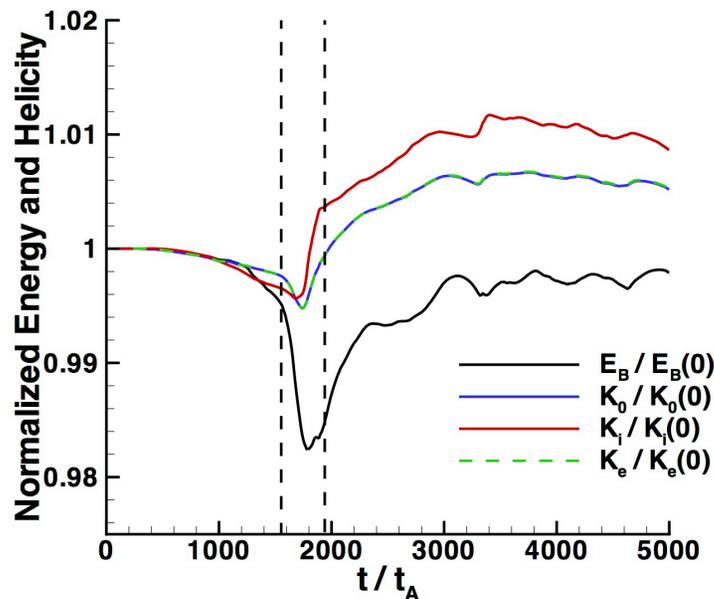
Magnetic energy and magnetic, ion, and electron helicities normalized by initial values are plotted from computations without (left) and with (right) an initial parallel flow profile.

Summary and Discussion of Two-Fluid RFP Relaxation

- Our two-fluid simulations show significant Hall dynamo activity during relaxation events.

- Parallel flow profiles change in the direction of the parallel Lorentz force-density from magnetic fluctuations.

- This result is inconsistent with observations from MST.

- Despite relative species-helicity conservation, the result does not show the flattening of the parallel flow profile predicted by two-fluid relaxation theory.

- Computations with no-slip boundary conditions and computations with free-slip conditions and pinch flow are not mechanically isolated.

- See poster JP8.00123 by Sauppe, Tuesday afternoon.

Non-inductive startup in Pegasus: Localized sources inject current filaments / magnetic flux ropes.

- Like early experiments on CDX and CCT, non-inductive startup in the Pegasus spherical torus uses localized injectors.

Visible-light images from Pegasus in filament, sheet, and diffuse operation. (Eidietis, JFE)
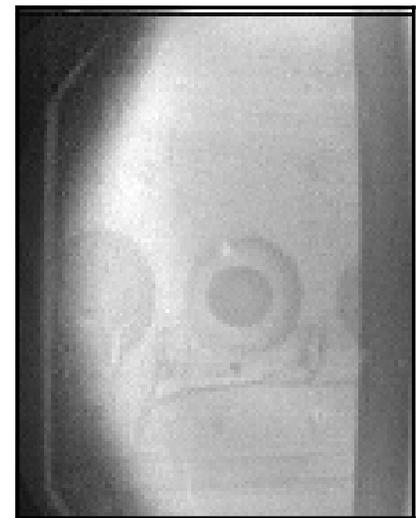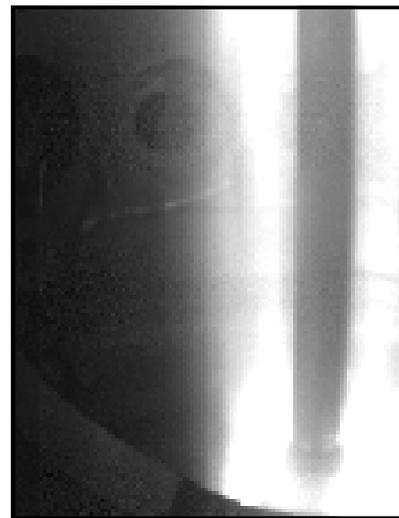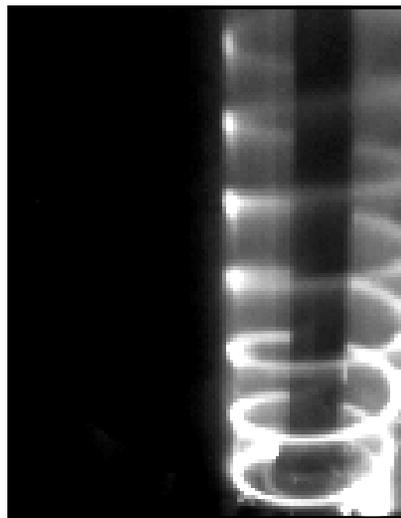
- Pegasus results with the divertor-injector configuration established distinct-filament, sheet, and diffuse tokamak-like discharges [N. W. Eidietis, J. Fusion Energy **26**, 43 (2007)].

- The more recent outboard-injector configuration includes PF induction for force-balance and additional current drive [Battaglia, NF **51** 073029 (2011)].

Our modeling simplifies the injectors, making them localized volumetric sources of helicity and heat.

- We focus on basic flux-rope dynamics and consider the first Pegasus configuration with a single source and without PF induction.

- In the experiment, DC voltage is applied from the plasma-injector aperture to an anode plate or the tank.

  - Magnetic helicity is injected via the surface contribution $-2 \oint \chi \mathbf{B} \cdot d\mathbf{S}$.

- Our simulations model the injectors with a localized source $\mathbf{E}_{inj} = \eta \mu_0^{-1} \lambda_{inj} \mathbf{B}$ in Ohm's law, oriented parallel to the desired current direction, to source helicity $+2 \int \mathbf{E}_{inj} \cdot \mathbf{B} \, dVol$.

- Localized ion heat is also applied.
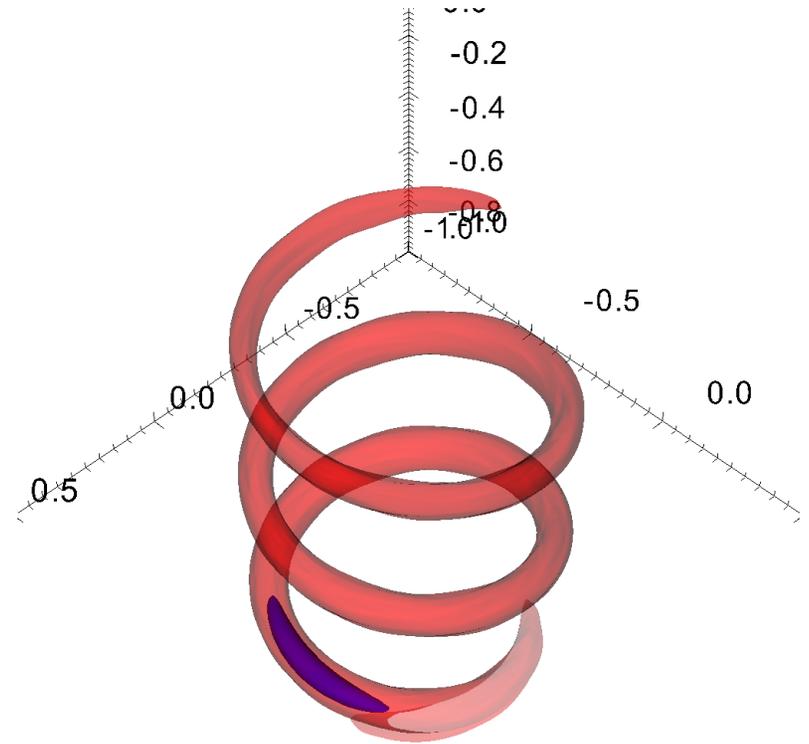
Isosurface of simulated $\lambda = \mu_0 J_{\parallel}/B$ at low injection levels with dark shading in the source-density region.

As plasma current builds, the activity and path of the rope change qualitatively.

Toroidal plasma current from MHD computation
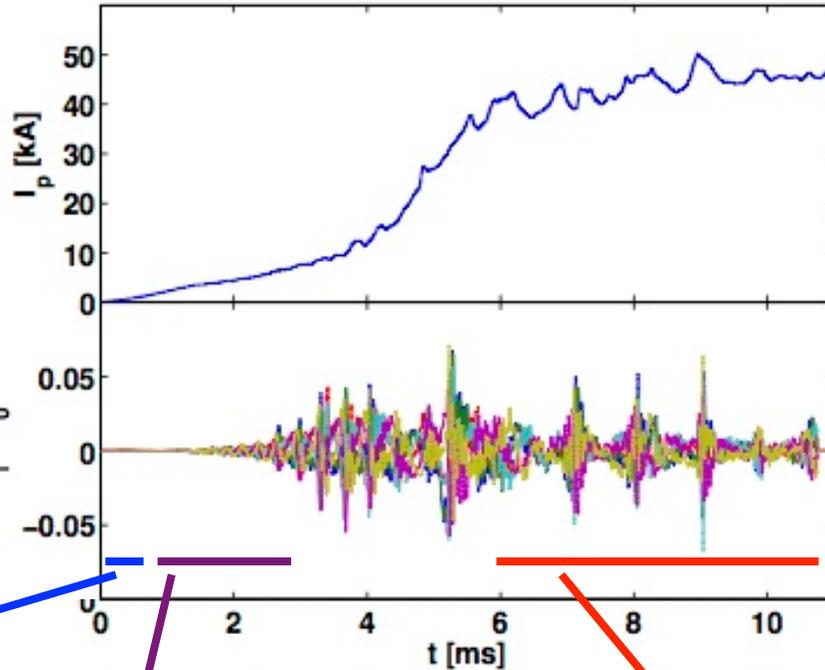
Relative magnetic fluctuations measured near midplane
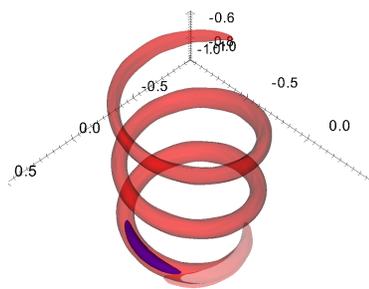
initial current path
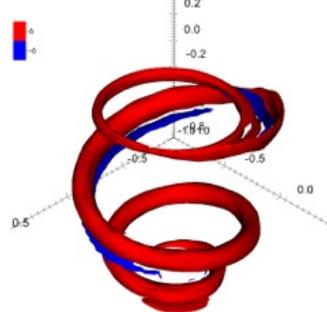
early ring formation
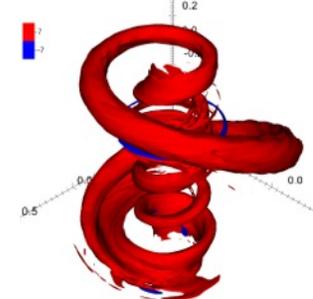
toroidal winding

Vacuum-field winding that directs the flux rope to have multiple passes leads to island-coalescence behavior.

Parallel current from the early phase of a Pegasus simulation.

- Pegasus ropes are neither periodic nor sinusoidal.
- Merging of different passes leads to ring formation. [O'Bryan, PoP **19**, 080701.]

Sketches from Finn&Kaw, PF 20, 72 (1977) for a periodic system.

- Multiple passes are required for relaxation into diffuse discharges [Eidietis, PhD thesis].

The formation of flux-rope rings in our simulations requires magnetic reconnection.

- Parallel current density in the direction opposite to the injected current is induced as different passes of the flux rope merge.

- The orientation of merging passes is necessarily *co-helicity*.
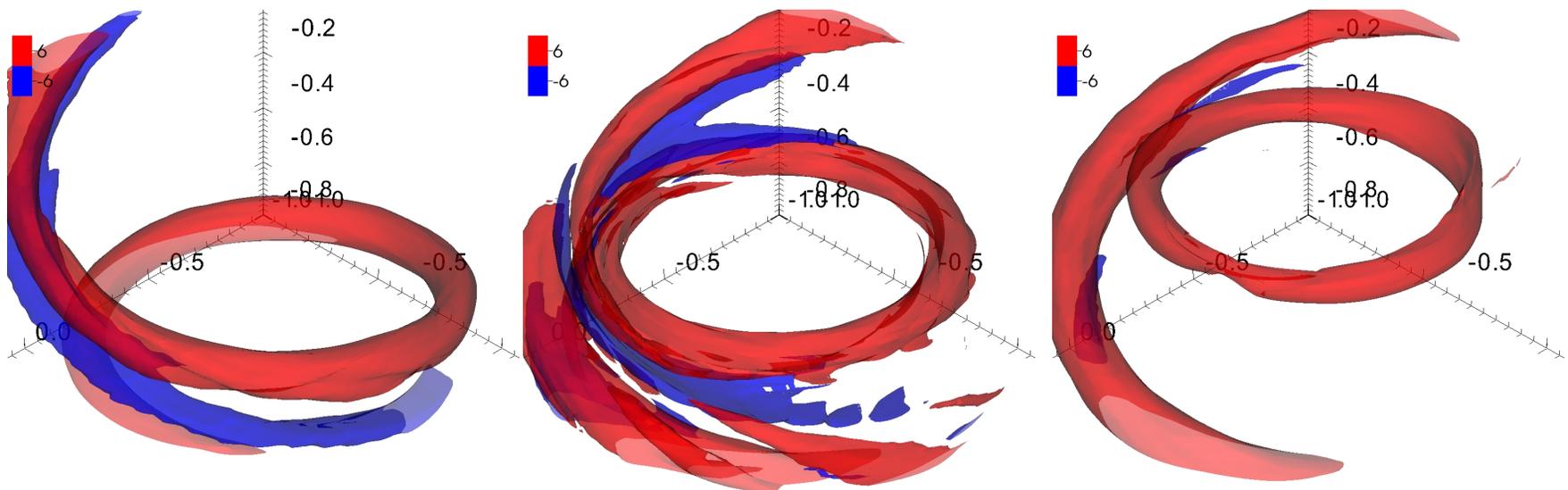
Isosurfaces of $\lambda=\mu_0 J_{||}/B$ during an early ring-formation event in the MHD simulation. Red is positive (parallel), and blue is negative (anti-parallel), and frames show intervals that are separated by 30 μs, starting at 2.63 ms.

Net poloidal flux accumulates over a sequence of ring formation events.
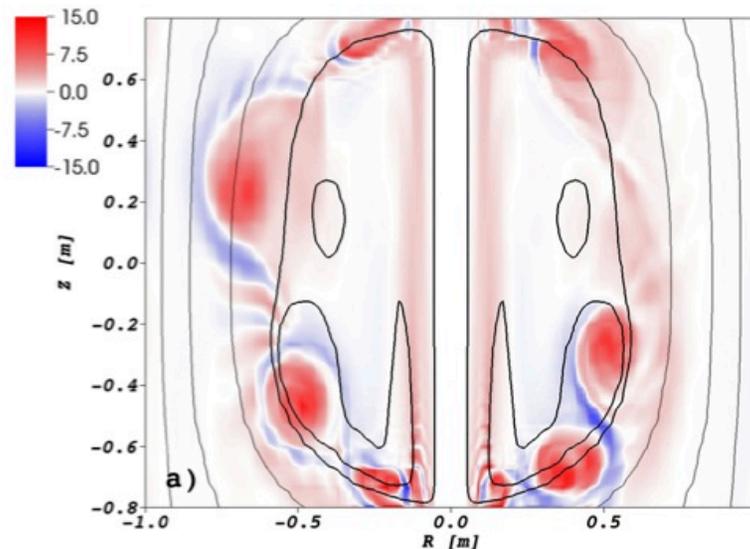
Contour lines of toroidally averaged poloidal flux superposed on contours of λ when I_p = 26 kA.
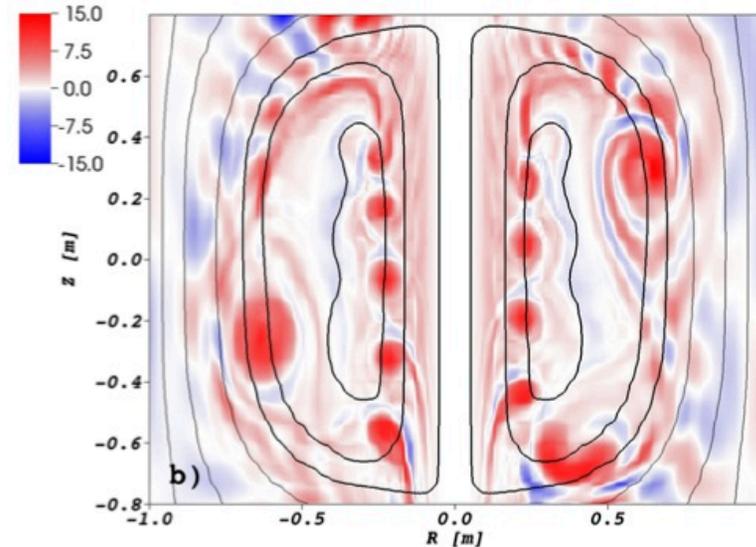
Contours of poloidal flux and λ when I_p = 42 kA.

- Significant poloidal flux amplification (relative to vacuum) occurs after reversal of large-scale poloidal field [O'Bryan, PoP **19**, 080701 (2012)].

Our helicity source induces net poloidal flux directly, but dynamo-like activity affects the global distribution.

- Our source has $\oint \mathbf{E}_{inj} \cdot \hat{\phi} R \, d\phi \neq 0$, so we are not modeling all of the current-drive processes in the experiment.

- The directly induced flux in the simulation is localized to the source region.

- MHD $-\left\langle \tilde{\mathbf{V}} \times \tilde{\mathbf{B}} \right\rangle$ and Hall $(ne)^{-1} \left\langle \tilde{\mathbf{J}} \times \tilde{\mathbf{B}} \right\rangle$ dynamo effects from the correlation of fluctuations can redistribute poloidal flux.

- Poynting's theorem can be applied to the toroidally averaged magnetic field. For low-frequency dynamics:

$$\frac{1}{2\mu_0} \frac{\partial}{\partial t} \left\langle \mathbf{B} \right\rangle^2 + \frac{1}{\mu_0} \nabla \cdot \left[\left\langle \mathbf{E} \right\rangle \times \left\langle \mathbf{B} \right\rangle \right] = -\left\langle \mathbf{E} \right\rangle \cdot \left\langle \mathbf{J} \right\rangle$$

  - Energy density in the mean field increases where $\left\langle \mathbf{E} \right\rangle \cdot \left\langle \mathbf{J} \right\rangle < 0$.

- With $\delta_i \approx 10$ cm and $\rho_s \approx 3$ cm at or below the simulated flux-rope diameter, and $\delta_\eta \approx 2$ cm, two-fluid effects are expected to be important.

The MHD dynamo effect induces ring current, while the Hall dynamo effect occurs on smaller scales.
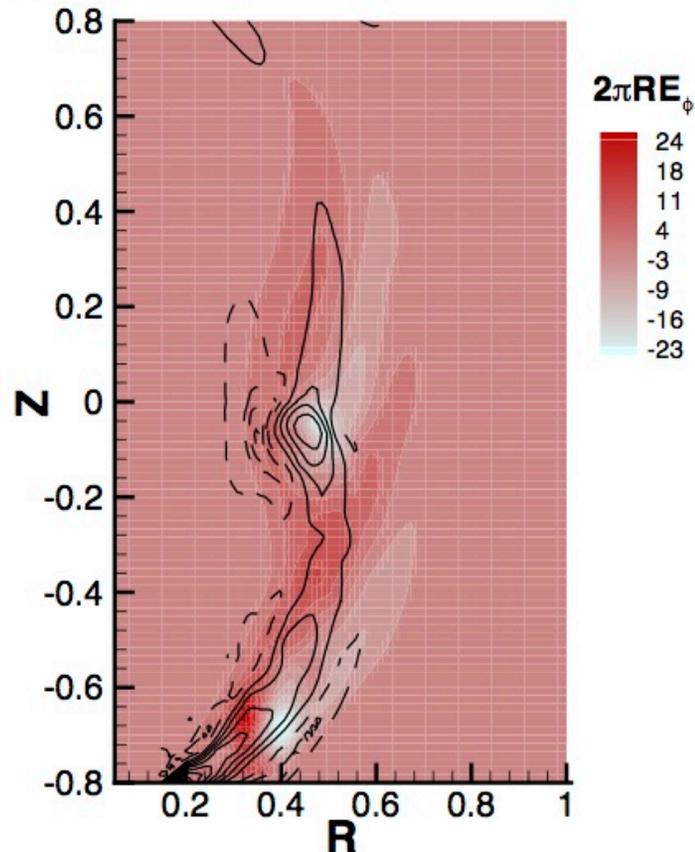
Contour lines of $\langle J_\phi \rangle$ overlaid on contours of emf from $-\langle v \times b \rangle$ during a ring formation event in the two-fluid simulation.
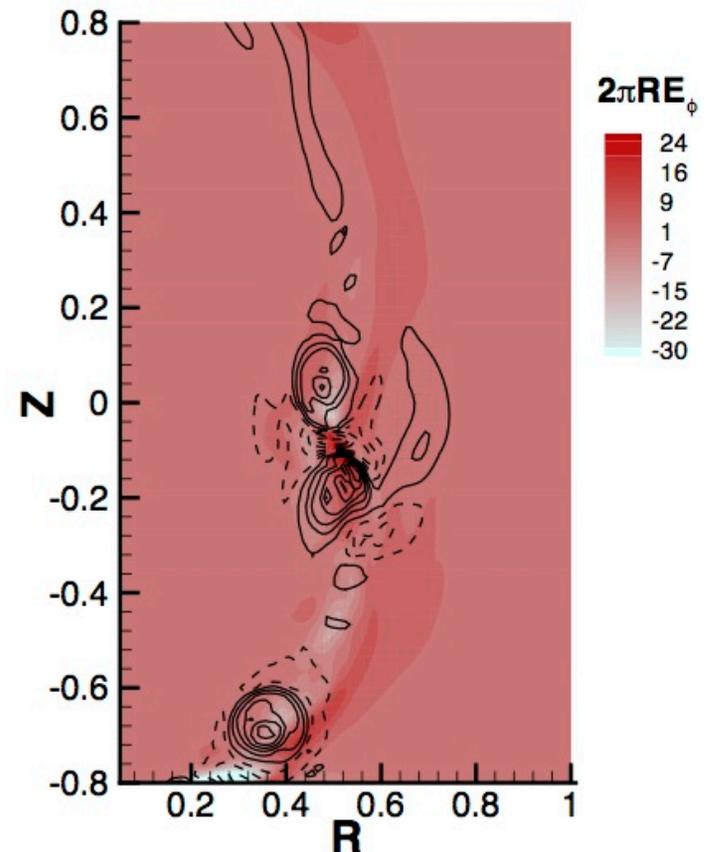
Contour lines of λ overlaid on contours of emf from $\langle j \times b \rangle$.

- The MHD dynamo effect supplies power to the ring.
- The Hall dynamo effect acts on a scale that is smaller than the ring.

Conclusions from the Pegasus Study

- Ring formation from co-helicity merging may be unique for tokamak startup configurations due to toroidal equilibrium considerations.

- MHD dynamo effect is evident in ring formation and is associated with rotation of a helical ring into a horizontal plane.

- Whether flux ropes survive late in the experiment's current injection will be determined by new diagnostics.

- See contributed talk JO4.00003 by John O'Bryan, 2:24 PM, Tuesday.

Concluding Remarks

- The varied parameter regimes of two-fluid modeling makes comprehensive verification more challenging than for single-fluid modeling.

- Our experience is that incomplete modeling (for example, dropping magnetization heat) may destabilize modes that are stable physically.

- Two-fluid modeling is proving to be important in our RFP and ST startup studies.

- We are also applying two-fluid modeling in tokamak studies of ELMs, RMPs, and sawteeth.